Combinatorial activities of Smad2 and Smad3 regulate mesoderm formation and patterning in the mouse embryo

N. Ray Dunn, Stéphane D. Vincent, Leif Oxburgh, Elizabeth J. Robertson* and Elizabeth K. Bikoff

Department of Molecular and Cellular Biology, Harvard University, 16 Divinity Avenue, Cambridge MA 02138, USA
*Author for correspondence (e-mail: ejrobert@fas.harvard.edu)

Accepted 7 January 2004

Development 131, 1717-1728
Published by The Company of Biologists 2004
doi:10.1242/dev.01072

Summary

TGFβ/activin/Nodal receptors activate both Smad2 and Smad3 intracellular effector proteins. The functional activities of these closely related molecules have been extensively studied in cell lines. We show both are expressed in the early mouse embryo from the blastocyst stage onwards and mediate Foxh1-dependent activation of the *Nodal* autoregulatory enhancer in vitro. Genetic manipulation of their expression ratios reveals that Smad3 contributes essential signals at early post-implantation stages. Thus, loss of *Smad3* in the context of one wild-type copy of *Smad2* results in impaired production of anterior axial mesendoderm, while selective removal of both *Smad2* and *Smad3* from the epiblast additionally disrupts specification of axial and paraxial mesodermal derivatives. Finally, we demonstrate that *Smad2*;*Smad3* double homozygous mutants entirely lack mesoderm and fail to gastrulate. Collectively, these results demonstrate that dose-dependent Smad2 and Smad3 signals cooperatively mediate cell fate decisions in the early mouse embryo.

Key words: Mesoderm induction, Smad2/3, Axis patterning, Nodal, Mouse

Introduction

Members of the Transforming Growth Factor β (TGFβ) superfamily of secreted growth factors regulate numerous embryonic processes, from axis formation and mesoderm patterning to allocation of the germline (reviewed by Hogan, 1996; Whitman, 1998; Zhao, 2003). In vivo the functions of these ligands are often dose dependent. For example, heterozygous mice carrying one copy of a null allele of *Bmp4* or *Bmp5* display a variety of phenotypic abnormalities (Dunn et al., 1997; Green, 1968). Moreover, several TGFβ family members are thought to provide key positional information by establishing morphogen gradients. In zebrafish, the Nodal-related molecule squint can act in a concentration-dependent manner and at a distance to activate target genes (Chen and Schier, 2001). Within the extracellular spaces, ligand concentration may be further refined by associations with various antagonists and co-factors and via specific protease activities (reviewed by Balemans and Van Hul, 2002). Precisely how distinct target cell populations convert local TGFβ signals into specific downstream responses has been the subject of intense investigation.

Previous studies have described dose-dependent functions for the TGFβ ligand Nodal and Smad2 (Madh2 – Mouse Genome Informatics), its cognate downstream effector, in coordinating cell fate specification and cell movements during early vertebrate development (Nomura and Li, 1998; Norris et al., 2002; Schier and Shen, 2000; Vincent et al., 2003; Whitman, 2001). In mouse, *Nodal* is expressed throughout the epiblast prior to gastrulation and then becomes rapidly confined to the posterior side of the embryo, marking the site of primitive streak formation (Conlon et al., 1994; Varlet et al., 1997). Genetic studies have shown that *Nodal* expression in the epiblast is essential for maintaining reciprocal tissue interactions that assign early embryonic polarity. Nodal signals to the overlying visceral endoderm (VE) where it activates Smad2 and promotes formation of the anterior visceral endoderm (AVE). This specialized signaling center first appears within a distal patch of VE and establishes proximodistal (PD) polarity within the early epiblast, and then emerges via directed cell movements as the early anterior organizer, converting initial PD polarity into the definitive embryonic anteroposterior (AP) axis. At the same time, Smad2-independent Nodal signaling within the epiblast is required to induce posterior markers (Brennan et al., 2001). Thus, *Nodal* mutant embryos arrest at the egg cylinder stage, failing to form either the AVE or primitive streak and therefore entirely lacking AP identity (Brennan et al., 2001; Conlon et al., 1991; Conlon et al., 1994).

The primitive streak normally becomes visible at embryonic day (E) 6.5 when cells on the posterior side of the epiblast ingress and emerge as mesoderm and definitive endoderm. Cells entering the streak adopt different fates depending on their position relative to the PD axis. Proximal epiblast cells give rise to extra-embryonic mesoderm. Cells at intermediate levels give rise to heart, lateral plate and paraxial mesoderm precursors, while more distal populations generate the axial mesendoderm (AME) and the node (reviewed by Lawson, 1999). At early to mid-streak stages, a discrete subpopulation of epiblast cells that exhibits classical ‘organizer’ activity, i.e. the ability to induce a secondary axis following heterotopic transplantation (reviewed by Camus and Tam, 1999), gives rise to the anteriormost AME, which comprises the prechordal plate (PCP) and anterior definitive endoderm (ADE) (Camus et al., 2000; Lawson, 1999). During gastrulation, the

progenitors of the PCP and ADE displace the VE and migrate anteriorly to underlie the neural plate, where they produce secondary inductive cues that reinforce the initial anterior identity established by the AVE (Rubenstein et al., 1998; Stern, 2001). Graded Nodal signals within the epiblast and the primitive streak have been shown to govern specification of the AME. For example, recent studies have shown that reducing *Nodal* expression within the mouse epiblast with partial loss-of-function *Nodal* alleles selectively disrupts specification of the anterior AME and consequently mutant embryos display varying degrees of anterior truncations (Lowe et al., 2001; Norris et al., 2002; Vincent et al., 2003).

TGFβ cell-surface receptors activate downstream intracellular effectors, the so termed R-Smads, that in turn associate with the co-mediator Smad4. This heteromeric complex translocates into the nucleus to regulate cell type-specific target gene expression (reviewed by Massagué and Wotton, 2000). Smad1, Smad5 and Smad8 function downstream of BMP sub-family ligands, whereas TGFβ/Activin/Nodal receptors activate the closely related Smad2 and Smad3 proteins (Moustakas et al., 2001; Shi and Massagué, 2003). Nodal signaling via the Alk4 or Alk7 type I receptor in association with either the ActRIIA or ActRIIB type II receptor has been shown to activate Smad2 (Kumar et al., 2001; Reissmann et al., 2001; Whitman, 2001). Interestingly, the closely related intracellular effector molecule Smad3 (Madh3 – Mouse Genome Informatics) shares an overall 92% amino acid identity with Smad2, and both Smad2 and Smad3 induce expression of dorsal mesodermal markers in *Xenopus* explant assays (Baker and Harland, 1996; Chen et al., 1997; Graff et al., 1996). Moreover, both Smad2 and Smad3 efficiently interact with the transcription factor Foxh1 (FAST) in vitro (Labbé et al., 1998; Yeo et al., 1999). These findings suggest that for a broad spectrum of in vivo functions, Smad2 and Smad3 are functionally interchangeable and that Smad3 also functions downstream of the Nodal receptor complex.

However, the N-terminal Smad2 MH1 domain contains a distinctive thirty amino acid insert predicted to impose steric constraints that selectively disrupt DNA binding (Shi et al., 1998). Consistent with this DNA-binding difference, Smad2 and Smad3 exhibit distinctive functional activities in a variety of transcriptional reporter assays (reviewed by Liu, 2003; Moustakas et al., 2001; Shi and Massagué, 2003). For example, Smad3 suppresses whereas Smad2 activates the *Xenopus goosecoid* promoter (Labbé et al., 1998). These findings suggest that Smad2 and Smad3 also play unique roles in directing cell type-specific responses. Consistent with this, *Smad2* and *Smad3* mutant mice exhibit strikingly different phenotypes. *Smad3*-deficient mice develop to term and exhibit only subtle developmental abnormalities (Datto et al., 1999; Yang et al., 1999; Zhu et al., 1998). We have previously shown that *Smad2* and *Smad3* expression domains mostly overlap at early embryonic stages (Tremblay et al., 2000). However *Smad3* is not expressed in the VE, where *Smad2* functions uniquely to specify the AVE. Thus, *Smad2* mutant embryos fail to form the AVE, display early patterning defects, and consequently become highly disorganized by E6.5 (Brennan et al., 2001; Heyer et al., 1999; Waldrip et al., 1998).

To further dissect shared and/or unique roles provided by Smad2 and Smad3, we have manipulated their expression ratios in vivo. We find that *Smad2*;*Smad3* double heterozygous animals are born at the expected Mendelian ratio and are fully viable and fertile. However, loss of *Smad3* in the context of one wild-type copy of *Smad2* results in embryonic lethality around E9.5. As for conditional loss of *Smad2* from the epiblast (Vincent et al., 2003), these $Smad2^{+/-}$;$Smad3^{-/-}$ mutant embryos display impaired production of anterior AME during gastrulation. Surprisingly, selective removal of both *Smad2* and *Smad3* from the epiblast disrupts specification of axial and paraxial mesodermal derivatives. Finally, we demonstrate that *Smad2;Smad3* double homozygous mutants entirely lack mesoderm and fail to gastrulate. The present work reveals for the first time that *Smad3* expression contributes essential signals at early post-implantation stages of mouse development.

Materials and methods

Mouse lines and genotyping

The genotyping assays and genetic backgrounds for the $Smad2^{Robm1}$ and $Smad2^{CA}$ targeted alleles were as described (Vincent et al., 2003; Waldrip et al., 1998). Congenic C57BL/6-*Smad3* heterozygous null animals (Datto et al., 1999) were outcrossed onto ICR (Taconic). The *Smad3* targeted null allele is denoted as $Smad3^{null}$ in this report, and was detected by PCR analysis of DNA from tail biopsies or embryonic fragments with primers: com, 5′-CTCCAGAGTTAAAAGCG-AAGTTCG-3′; wt, 5′-AAAATGCTGCACGGAAGCCAGGTC-3′; and neo, 5′-ATTTGTCACGTCCTGCACGACG-3′. The wild-type and mutant PCR products are 489 and 347 bp, respectively. The *Sox2Cre* transgene was detected as described (Vincent et al., 2003).

Whole-mount in situ hybridization and histology

Individually genotyped or groups of embryos were processed for whole-mount in situ hybridization as described (Nagy et al., 2003) with the following probes: *Foxa2*, *Shh*, *T*, *Sox2*, *Meox1*, *Bmp4*, *Oct4* (*Pou5f1* – Mouse Genome Informatics), *Otx2*, *Six3*, *Fgf8*, *Krox20* (*Egr2* – Mouse Genome Informatics), *Chrd*, *Nog*, *Cer1*, *Hex*, or *Smad3* (IMAGE clone 45861). For histology, embryos or decidua were fixed in 4% paraformaldehyde, dehydrated through an ethanol series, and embedded in paraffin wax. Hematoxylin and eosin staining was performed according to standard protocols.

Protein purification and western blotting

Protein extracts (50 μg) derived from CCE ES cells, KT15 $Smad2^{Robm1}$ homozygous ES cells, STO fibroblasts, or thymi, spleen and livers of adult mice were mixed with an equal volume of 2×Laemmli buffer and then separated on a 10% SDS-PAGE gel followed by transfer to nitrocellulose (Protran). Blots were incubated with either mouse anti-Smad2/3 (Transduction) or rabbit anti-Smad3 (Zymed) primary antibodies (Abs) and then with either anti-mouse or anti-rabbit IgG HRP-conjugated secondary Abs (Amersham). Blots were developed by chemiluminescence using ECL (Amersham).

Plasmids and transfections

N-terminally FLAG-tagged human *Smad2* and *Smad3* cDNA cassettes (Yagi et al., 1999) were subcloned into pCAGGS (Niwa et al., 1991). Mv1Lu mink lung cells (ATCC) were grown overnight prior to transfection with a total of 1.5 μg DNA complexed with Lipofectamine 2000 (Invitrogen). The following plasmids (0.25 μg/well) were used in transfections: $(n2)_7$-luc, caALK4, pCR3-FAST2, pcDNA3-Smad4myc, pCAGGS-FLAG-hSmad2 and pCAGGS-FLAG-hSmad3, and the renilla luciferase expression vector pRL-CMV (Promega). Cell lysates were analyzed after 40 hours using the Dual-Luciferase Reporter Assay System (Promega). Mean values of each set of triplicates were plotted as fold induction compared to activation of the reporter by caALK4 alone. FLAG-hSmad2 or FLAG-hSmad 3 protein expression was verified by western analysis with the

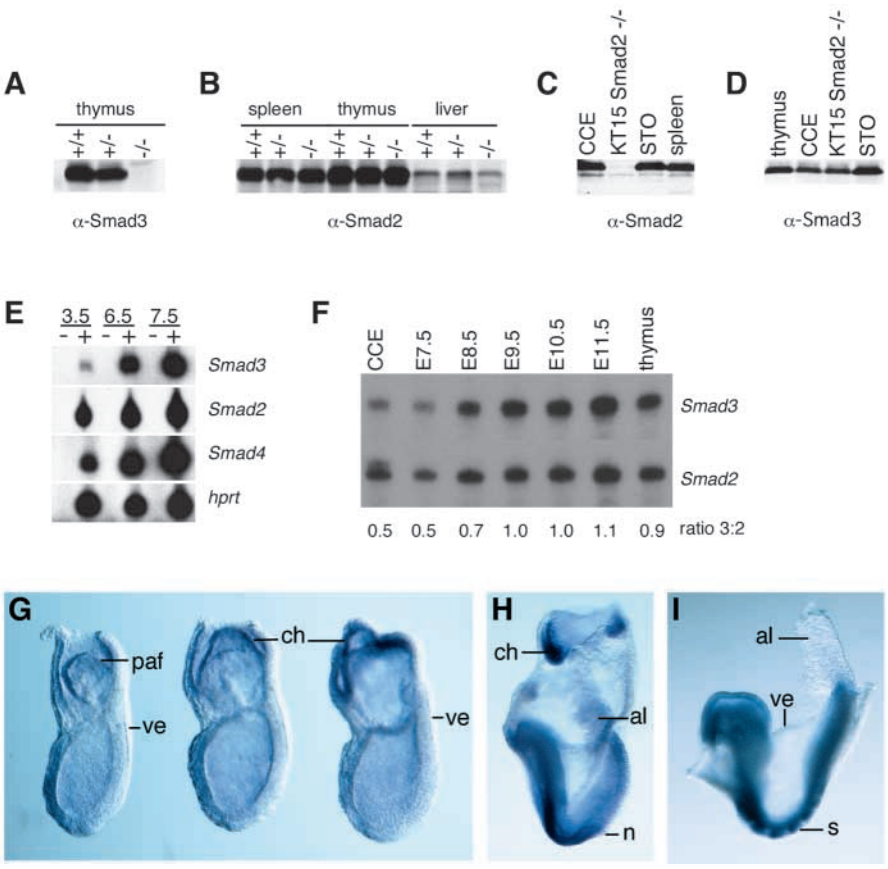

Fig. 1. *Smad2* and *Smad3* are independently regulated and co-expressed in the early embryo. (A-D) Western blot analysis of adult organ and cell lines. (A) Thymus extracts from homozygous *Smad3*^{null} animals (–/–) lack detectable Smad3 protein. (B) Equivalent Smad2 protein levels are found in wild-type, *Smad3*$^{+/–}$ and *Smad3*$^{–/–}$ spleen, thymus and liver extracts. (C) CCE ES cells, STO fibroblasts and spleen express Smad2 protein, whereas KT15 *Smad2*^{Robm1} homozygous ES cell lines contain no Smad2. (D) Similar Smad3 levels are observed in thymus, CCE and KT15 Smad2-deficient ES cells, and STO fibroblasts. (E) Semi-quantitative RT-PCR analysis of *Smad3*, *Smad2*, *Smad4* and hypoxanthine phosphoribosyltransferase (*Hprt*) expression in blastocysts (E3.5) and gastrulation stage embryos (E6.5 and 7.5). *Smad2*, *Smad3* and *Smad4* are co-expressed at all stages examined. (F) Quantitative analysis of *Smad2* and *Smad3* expression levels by ribonuclease protection assay of CCE ES cell, embryo and adult thymus total RNA. *Smad2* transcripts are approximately twofold more abundant than *Smad3* transcripts in ES cells and E7.5 embryos. *Smad3* levels equalize with *Smad2* as development progresses, and by E10.5/11.5 the ratio of *Smad3*:*Smad2* transcripts is nearly 1:1. (G-I) *Smad3* whole-mount in situ hybridization. (G) Mouse embryos at mid- to late primitive streak stages show low levels of *Smad3* expression throughout the embryo. The highest level of expression is seen in the extra-embryonic ectoderm of the posterior amniotic fold (paf) and its later derivative the chorion (ch). The visceral yolk sac endoderm (ve) is negative for *Smad3*. (H,I) *Smad3* expression levels increase within the embryo proper by the early somite stage (E8.0-8.5), and are observed in the midline, node (n) and somites (s).

M5 anti-FLAG mouse monoclonal. Supernatant from the 9e10 hybridoma (ATCC) was used to detect Smad4myc. Anti-mouse IgG HRP (Amersham) was used to detect bound primaries.

RT-PCR and ribonuclease protection assays

Total RNA from CCE ES cells, thymus or wild-type embryos was prepared using the Trizol® method (Invitrogen). Ribonuclease protection assays were performed on 10 μg total RNA (RPA III™ kit, Ambion). The *Smad2* probe corresponds to a 3′ 221 bp *Bgl*II-*Bam*HI fragment (Waldrip et al., 1998), and the *Smad3* probe represents a 3′ 237 bp *Hin*cII fragment.

Blastocyst RNA was isolated with the Absolutely RNA Microprep™ Kit (Stratagene). Random-primed total RNA was reverse transcribed with SuperScript™ reverse transcriptase (Invitrogen), and resulting cDNA assayed by RT-PCR for *Smad2* and *Hprt* (Oxburgh and Robertson, 2002), *Smad3* (Rosendahl et al., 2001) and *Smad4* expression in the presence of 1 μCi P^{32}-dCTP. *Smad4* RT-PCR reactions use forward primer 5′-GCCATTGGTTTTCACTGCCTTC-3′ and reverse primer 5′-GGGTGTTGG ATGGTTGAATCG-3′), and yield a 632 bp product.

RPA and RT-PCR products were separated on 5% PAGE gels, exposed to film and quantitated by phosphoimager.

Results

Absence of feedback regulation of Smad2 and Smad3 expression levels

Recent work suggests that feedback inhibition controls *Smad2* and *Smad3* expression ratios, and that in the absence of *Smad3*, *Smad2* expression is upregulated (Weinstein et al., 2001). To re-examine this possibility, we assessed Smad2/3 protein expression in different genetic contexts (Fig. 1). Smad2 protein levels are comparable among spleen, thymus and liver extracts from wild-type, *Smad3*$^{+/–}$ and *Smad3*$^{–/–}$ animals (Fig. 1B), and as a control no Smad3 protein is detectable in thymus extracts from adult *Smad3*^{null} homozygous mice (Fig. 1A) (Datto et al., 1999). We also find Smad3 protein at equivalent levels in wild-type CCE ES cells and KT15 ES cells that are homozygous for the targeted *Smad2*^{Robm1} loss-of-function mutation (Fig. 1D). Similar conclusions were reached analyzing Smad3 levels in wild-type and Smad2-deficient embryo extracts at E8.5 (data not shown). Taken together, these results strongly argue that *Smad2* and *Smad3* expression is independently regulated.

Restricted tissue-specific *Smad3* expression in the early embryo

Smad2 and *Smad3* expression patterns have been compared at mid- to late gestation stages (Flanders et al., 2001; Tremblay et al., 2000). However, the onset of *Smad2* and *Smad3* expression has not been previously documented. To evaluate this we performed semi-quantitative RT-PCR experiments. We find that both *Smad2* and *Smad3* as well as *Smad4* transcripts are expressed from the blastocyst stage onwards (Fig. 1E). *Smad2* and *Smad3* expression ratios were also compared via

RNAse protection assays (RPA). Results shown in Fig. 1F demonstrate that *Smad2* transcripts are present at approximately two-fold higher levels in ES cells and at the earliest embryonic stage examined (E7.5). However, *Smad2* and *Smad3* are co-expressed at roughly equivalent levels beginning at E8.5.

Smad3 expression domains were further analyzed by whole-mount in situ hybridization. Consistent with previous results, *Smad2* is broadly expressed throughout all tissues and at all stages analyzed (de Sousa Lopes et al., 2003; Tremblay et al., 2000; Waldrip et al., 1998). As expected, the visceral endoderm lacks *Smad3* transcripts, but *Smad3* is expressed throughout the epiblast (Fig. 1G) (Tremblay et al., 2000). At early gastrulation stages, *Smad3* transcripts are most abundant in the extra-embryonic ectoderm and later in its derivative the chorion (Fig. 1G,H). Highest levels of *Smad3* expression are seen along the ventral midline and in the somites by E8.5 (Fig. 1I).

Both Smad2 and Smad3 activate the *Nodal* ASE

Both Smad2 and Smad3 associate with the activated Alk4 receptor and can propagate Nodal signaling in P19 embryonal carcinoma cells (Kumar et al., 2001; Lebrun et al., 1999). However, it remains unknown whether Smad2 and Smad3 both transduce Nodal/Alk4 signals in early mouse embryos. A Foxh1-dependent autoregulatory enhancer, termed the ASE, directs *Nodal* expression in the early epiblast, VE and left lateral plate mesoderm (Adachi et al., 1999; Norris et al., 2002; Norris and Robertson, 1999), and interestingly an ASE-*lacZ* reporter transgene is activated appropriately in the epiblast of *Smad2*-deficient embryos (Brennan et al., 2001). This observation suggests that Smad3 functionally compensates for the loss of Smad2 in this genetic context. To test this possibility directly, we compared the abilities of Smad2 and Smad3 to activate the $(n2)_7$-*luc* reporter construct containing seven tandem repeats of a Foxh1-responsive 24 bp oligonucleotide from the mouse *Nodal* ASE. This reporter is activated by Foxh1 in a TGFβ-dependent manner in Mv1Lu cells (Saijoh et al., 2000). As shown in Fig. 2A, in the presence of a constitutively active Alk4 receptor, both Smad2 and Smad3 give robust amplification of the transcriptional response. These results demonstrate that both Smad2 and Smad3 mediate Foxh1-dependent activation of the *Nodal* ASE.

Defective formation of AME in *Smad2*$^{+/-}$;*Smad3*$^{-/-}$ mutant embryos

The largely overlapping expression patterns of *Smad2* and *Smad3* in the early embryo, as well as their equivalent activation of the $(n2)_7$-*luc* reporter, suggest Smad2 and Smad3 function as co-effectors of Nodal signaling in vivo. To directly address this possibility, we intercrossed *Smad2*$^{Robm1/+}$ and *Smad3*$^{null/+}$ mice with the aim of modulating the relative intracellular levels of Smad2 and Smad3 in the embryo. Contrary to a previous report (Weinstein et al., 2001), *Smad2*$^{Robm1/+}$;*Smad3*$^{null/+}$ double heterozygous mice were recovered at the expected Mendelian ratios and are fully viable and fertile (data not shown). To further reduce *Smad3* expression levels, we next intercrossed *Smad2*$^{+/-}$;*Smad3*$^{+/-}$ and *Smad3*$^{+/-}$ mice. Interestingly, *Smad2*$^{+/-}$;*Smad3*$^{-/-}$ embryos fail to develop to term and can be grouped into two general classes by E9.5 according to the severity of their phenotype. A proportion of these mutants display anterior truncations, with

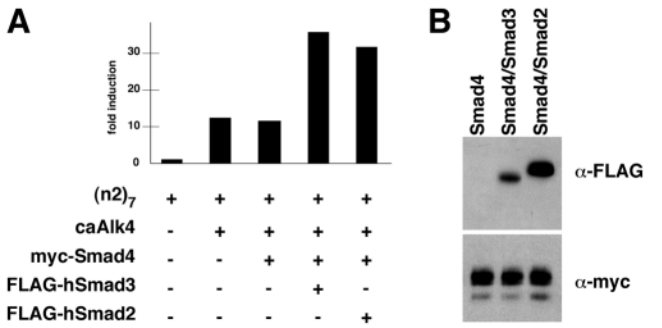

Fig. 2. Regulation of the Foxh1-dependent $(n2)_7$-*luc* reporter by Smad2 or Smad3. (A) The constitutively active Alk4 (caAlk4) Nodal receptor with or without mycSmad4 leads to modest upregulation of the $(n2)_7$-*luc* reporter in Mv1Lu cells. Addition of either FLAG-hSmad3 or FLAG-hSmad2 potentiates reporter activity to levels consistent with the previously demonstrated TGFβ-dependent regulation of $(n2)_7$-*luc* (Saijoh et al., 2000). (B) Western blot analysis of protein extracts from transfected cells confirms appropriate protein production of mycSmad4, FLAG-hSmad3 and FLAG-hSmad2 proteins.

accompanying loss of diagnostic structures such as the optic vesicle, fusion of the first branchial arch, enlarged pericardium, a disorganized heart tube and a rudimentary gut tube (Fig. 3D-F). More severely affected embryos remain in a lordotic position or are incompletely turned, fail to undergo ventral closure and show chaotic organization of midline structures, including gut, neural tube and somites (Fig. 3G,H). The anterior truncations frequently manifest as a miniaturized head-like structure, with the fused branchial arch outgrowth attaching itself to the enlarged pericardium (Fig. 3H).

These anterior defects could be caused by defective specification of or signaling by the AVE or the AME, or possibly both tissues. However, when a *Sox2Cre* transgene expressed exclusively in the epiblast was recently used in conjunction with the loxP-flanked *Smad2*^{CA} conditional allele, we found that selective loss of *Smad2* from this tissue prior to gastrulation does not prevent formation of the AVE, but rather eliminates the bulk of the definitive endoderm and severely disrupts the formation of anterior AME, resulting in tissue defects indistinguishable from those described above for *Smad2*$^{+/-}$;*Smad3*$^{-/-}$ embryos (Vincent et al., 2003). Collectively, these findings strongly argue that *Smad2* and *Smad3* activities within the epiblast act synergistically to specify the anterior AME progenitors during early gastrulation stages.

We used a panel of molecular markers to evaluate AME specification in *Smad2*$^{+/-}$;*Smad3*$^{-/-}$ mutant embryos. The winged helix transcription factor *Foxa2* (*Hnf3b*) is first expressed in the anterior primitive streak and AVE, then slightly later in the patent node, AME, notochord and floorplate (Fig. 4A,C,E). *Smad2*$^{+/-}$;*Smad3*$^{-/-}$ embryos show *Foxa2* expression within the AVE and node, but very little to no expression is detected in the region of the AME that normally extends rostrally from the node (Fig. 4B,D,F). *Shh* is also expressed in the node, AME and notochord (Fig. 4G,I,K), but in mutant embryos *Shh* transcripts are limited to the node and notochord, with only occasional *Shh*-positive AME cells being found in the presumptive anterior midline (Fig. 4H,J,L). Thus,

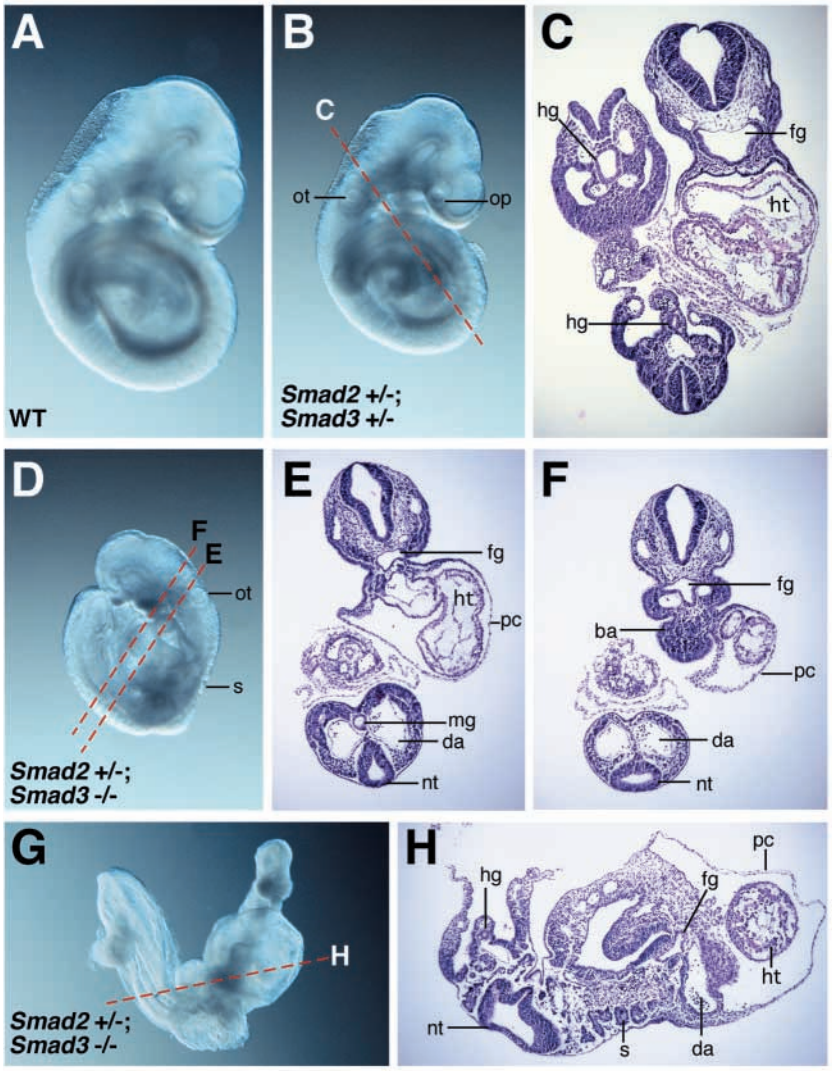

Fig. 3. Abnormalities in *Smad2*$^{+/-}$;*Smad3*$^{-/-}$ mutant embryos. Whole-mount views of E9.5 (A) wild-type (WT), (B) *Smad2*$^{+/-}$;*Smad3*$^{+/-}$ and (D,G) *Smad2*$^{+/-}$;*Smad3*$^{-/-}$ littermate embryos. (B) *Smad2*$^{+/-}$;*Smad3*$^{+/-}$ embryo with wild-type (A) morphology. (C) Transverse section of B. A moderately affected *Smad2*$^{+/-}$;*Smad3*$^{-/-}$ mutant embryo (D) completes turning, has reiterated somites (s) and an otic vesicle (ot), but lacks anterior-most neural structures, including forebrain and optic vesicle (op), and displays a mispatterned, enlarged heart (ht) within an expanded pericardium (pc). (E,F) Transverse sections of embryo in D reveal the presence of a gut tube along the length of the embryo, as well as a thickened anterior tissue mass probably resulting from fusion of the first branchial arches (ba). (G) A more severely affected mutant embryo fails to complete the turning sequence and to close the ventral body wall. Heart development is severely compromised, and anterior development is significantly diminished. (H) Transverse section of G shows a rudimentary gut tube, with chaotic development of neural and mesodermal structures along the body axis. da, dorsal aorta; nt, neural tube; fg, foregut; mg, midgut; hg, hindgut.

we conclude that the AME fails to form in *Smad2*$^{+/-}$;*Smad3*$^{-/-}$ mutant embryos.

The presence of a distinct node and its derivative the notochord reveals some degree of midline development in *Smad2*$^{+/}$;*Smad3*$^{-/-}$ mutant embryos. The BMP antagonists Noggin (Nog) and Chordin (Chrd) are diagnostic markers for the AME and node (Bachiller et al., 2000). In contrast to wild-type littermates at the headfold stage, mutant embryos show downregulated expression of *Nog* and *Chrd* in the midline, but expression is retained in the node region (Fig. 4N,P). These markers also identify the posterior PCP, and this expression domain is entirely absent in mutant embryos (Fig. 4N,P).

The definitive endoderm emerges either side of the midline as a thin, superficial layer of cells that displaces VE proximally, and is marked by expression of the Nodal/Wnt antagonist *cerberus* (*Cer1*) and *Hhex*. Expression levels of these two diagnostic markers are greatly diminished but not completely lost in the distal region of mutant embryos (Fig. 4Q,R), allowing us to conclude that ADE formation is significantly impaired. At E8.5, *Hhex*, which normally marks invaginating cells of the foregut pocket, is lost (Fig. 4T), and *Shh* expression in the hindgut pocket is significantly reduced compared with wild type (Fig. 4L′). At E9.5, we observe a rudimentary gut tube in *Smad2*$^{+/-}$;*Smad3*$^{-/-}$ mutants (Fig. 3E,F,H). The tissue occupying this region probably originates from extra-embryonic endoderm that fails to be displaced, as was previously shown in embryos that develop from an epiblast lacking *Smad2* (Vincent et al., 2003).

Similar to other reports describing defects in the specification or maintenance of the AME, *Smad2*$^{+/-}$;*Smad3*$^{-/-}$ mutant embryos are morphologically recognizable at the late headfold stage due to the development of a thickened anterior neuroepithelium (Fig. 4N,P) (Hallonet et al., 2002; Martinez Barbera et al., 2000; Shawlot et al., 1999). At E8.5, these embryos display a flattened neural region, with anterior truncations and fusions and persistent lack of neural groove (Fig. 4L,V,X,Z). Forebrain (*Six3* and *Otx2*), midbrain (*Fgf8* and *Otx2*) and hindbrain (*Krox20*) markers are induced (Fig. 4L,U-Z). Among the markers analyzed, only *Fgf8* expression in the anterior neural ridge, a forebrain organizing center within the anteriormost neural plate (Rubenstein et al., 1998), is consistently absent (Fig. 4Z), confirming loss of forebrain structures. Taken together, these results show that in *Smad2*$^{+/-}$;*Smad3*$^{-/-}$ mutants specification of the neural plate occurs normally, but the loss of anterior AME compromises its subsequent growth and patterning. Collectively, these experiments demonstrate that Smad2 and Smad3 signals cooperatively specify anterior streak fates.

Smad2 and *Smad3* co-expression within the epiblast is essential for mesodermal patterning

To further assess *Smad3* contributions during gastrulation and mesoderm patterning, the *Smad3* null allele was introduced into the *Smad2*^{CA} conditional background (Vincent et al., 2003). In embryos with *Smad2*-deficient epiblast but expressing one wild-

Fig. 4. Loss of anterior primitive streak derivatives in *Smad2*$^{+/-}$;*Smad3*$^{-/-}$ mutant embryos. Whole-mount in situ hybridization of (A,C,E,G,I,K,K′,M,O,S, U,W,Y) wild-type (WT) and (B,D,F,H,J,L,L′,N,P,T,V,X,Z) *Smad2*$^{+/-}$;*Smad3*$^{-/-}$ mutant (mut) embryos at (A,B,Q) E7.25, (C-J,R) E7.5, (M-P) E7.75 and (K-L,S-Z) E8.5. (A-F) *Foxa2* transcripts first identify the AVE (red line), then AME cells emerging from the anterior streak and later demarcate the node (n). (A,B) *Foxa2* and (Q) *Cer1* expression in the AVE confirms the normal establishment of the primary anteroposterior axis. However, mutant embryos show few (B) to no (D,F) *Foxa2*-expressing AME cells extending anteriorly. Similar results were obtained with *Shh* (G-J) that is also diagnostic for the AME and node. Note that *Foxa2* expression is retained in the patent node (D,F). In both control and mutant embryos at the early somite stage (K-L), *Shh* expression persists in the node and identifies its derivative the notochord (nc). At the early headfold stage, (M,N) *Nog* and (O,P) *Chrd* mark the node, midline and posterior PCP (bracket), and are downregulated and truncated anteriorly in mutant embryos (N,P). Note the expanded anterior neuroectoderm in N,P, and lack of neural groove in P. (Q,R) Lower levels of the nascent definitive endoderm markers *Cer1* and *Hhex* are observed during early gastrulation. At E8.5, *Hhex* marks involuting foregut endoderm and lateral angioblasts (ab) (S). Foregut *Hhex* expression is absent, but retained in angioblasts in mutant embryos (T). Similarly, *Shh* expression in the hindgut (hg) endoderm of mutants is largely lost (K′,L′). (U-X) The loss of anterior structures is revealed by diminished *Six3* and *Otx2* expression. (Y,Z) *Fgf8* is expressed in the anterior neural ridge (arrowhead) and mid/hindbrain boundary (asterisk) in the wild type. In mutant embryos, anteriormost *Fgf8* transcripts are absent, whereas expression in the mid/hindbrain region is normal (Z). (K,L) Hindbrain formation is unperturbed as assessed by *Krox20* expression in rhombomeres 3 and 5. (W-Z) Posterior *T* expression indicates ongoing gastrulation.

type copy of *Smad3* (*Sox2Cre*;*Smad2*$^{Robm1/CA}$;*Smad3*$^{null/+}$), all derivatives of the anterior primitive streak, including PCP, ADE, notochord, node and posterior endoderm are eliminated (Fig. 5B). The loss of axial structures is confirmed by the complete absence of *Shh* expression (Fig. 5D); similar results were obtained with *Foxa2* (Vincent et al., 2003). Somites, a derivative of paraxial mesoderm, are fused across the midline, a feature associated with the loss of the node and notochord (Fig. 5B,B′). Anterior development is compromised, and in some embryos the allantois is enlarged (Fig. 5B,D).

Next, we examined embryos lacking both *Smad2* and *Smad3* activities (*Sox2Cre*;*Smad2*$^{Robm1/CA}$;*Smad3*$^{null/null}$). Remarkably in the context of a *Smad2*-deficient epiblast, loss of *Smad3* activity severely compromises patterning of much of the

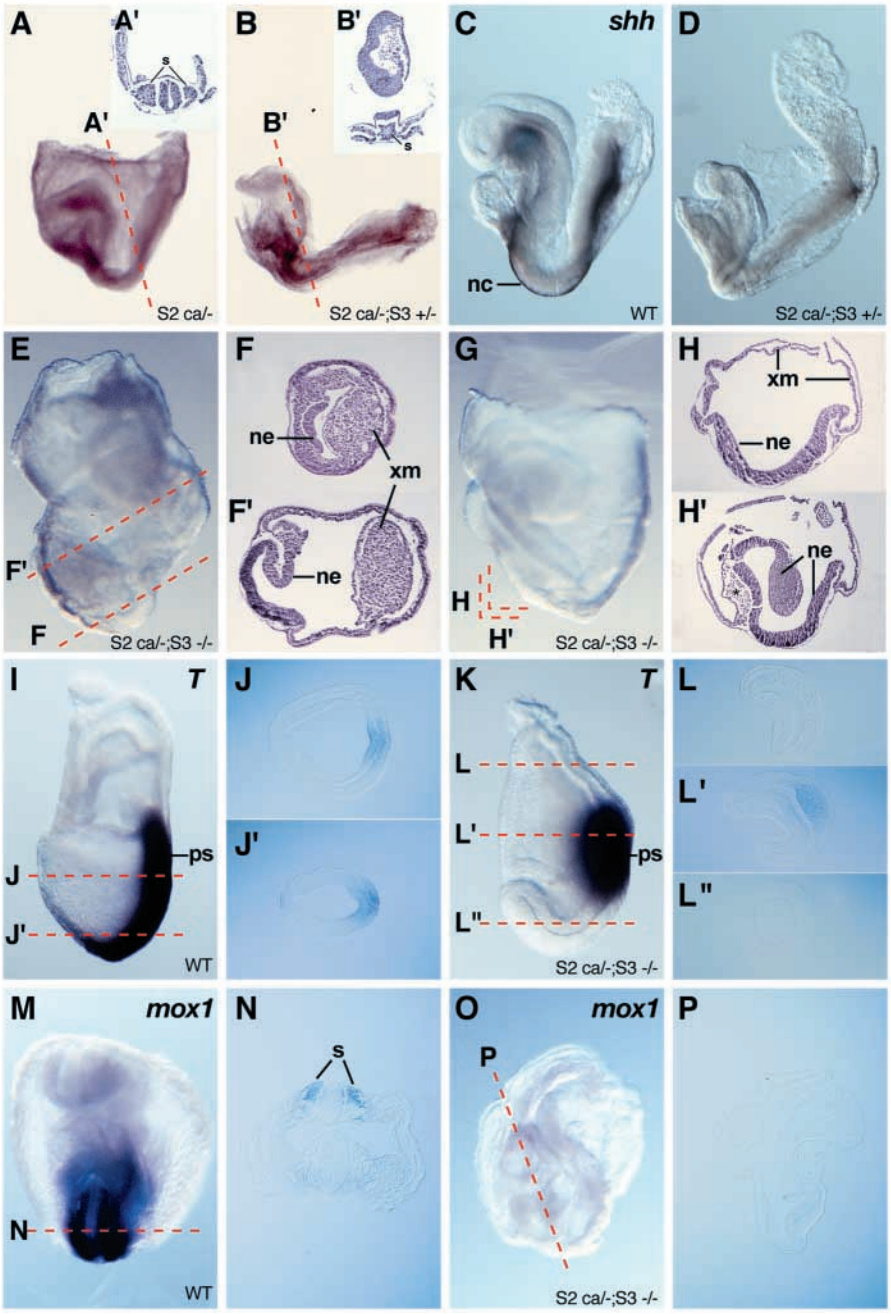

Fig. 5. Conditional removal of *Smad2* in the context of *Smad3* deficiency leads to gastrulation and streak patterning defects. Whole-mount views or sections as indicated of (A) *Sox2Cre*;*Smad2*$^{Robm1/CA}$ (S2 ca/-), (B-D) *Sox2Cre*;*Smad2*$^{Robm1/CA}$;*Smad3*$^{null/+}$ (S2 ca/-;S3$^{+/-}$), (E-H′,K-L″,O,P) *Sox2Cre*;*Smad2*$^{Robm1/CA}$;*Smad3*$^{null/null}$ (S2 ca/-;S3$^{-/-}$) and (I-J′,M-N) wild-type (WT) embryos at (I-L″) E7.5 and (A-H′,M-P) E8.5. (A) *Sox2Cre*;*Smad2*$^{Robm1/CA}$ mutants display anterior truncations similar to *Smad2*$^{+/-}$;*Smad3*$^{-/-}$ embryos and normal bilateral somites (s) (A′). (B) Combined reduction of *Smad3* gene dose to one wild-type allele and loss of *Smad2* in the epiblast leads to consistent anterior truncations and elimination of notochord (nc), node and definitive endoderm, which results in somite fusions across the midline (B′). (C,D) Failure to detect *Shh* transcripts by whole-mount in situ hybridization confirms absence of midline structures in *Sox2Cre*;*Smad2*$^{Robm1/CA}$;*Smad3*$^{null/+}$ mutants. (E-H′) Combined loss of *Smad2* and *Smad3* in the epiblast significantly impacts mesoderm formation and patterning. Mutant embryos are mainly composed of neuroectoderm (ne). (I-L″) *T* expression in the presumptive posterior marks nascent mesoderm forming in the primitive streak (ps). However, production of embryonic mesoderm is greatly diminished, as evidenced by restricted *T* expression and absence of the paraxial mesoderm marker *Meox1* (M-P). Small pockets of presumptive heart mesoderm are occasionally observed. By contrast, extra-embryonic mesoderm (xm) is formed, lining the visceral yolk sac and forming a compact structure resembling an allantois (F-H′).

primitive streak. At E8.5, *Sox2Cre*;*Smad2*$^{Robm1/CA}$;*Smad3*$^{null/null}$ embryos have distinct embryonic and extra-embryonic regions (Fig. 5E,F′). The embryonic region largely comprises folded neuroepithelial tissue that resembles a primitive neural axis (Fig. 5E-H′) and broadly expresses *Hesx1* (data not shown). Gastrulation initiates, as evidenced by the expression of *T* in the posterior region at E7.5, but mesoderm formation is greatly impaired (Fig. 5I,K). Neither *T*-positive axial mesodermal nor *Meox1*-positive paraxial mesodermal populations are specified (Fig. 5I-P). However, a small pocket of mesoderm is often observed in the presumptive heart region at E8.5 (Fig. 5H′). Thus, co-expression of *Smad2* and *Smad3* within the epiblast is required for correct induction and patterning of mesodermal cell types along the anteroposterior axis of the primitive streak. Highest levels of *Smad2/3* activity are required for formation of a subset of anterior streak derivatives, i.e. the AME. Intermediate loss of *Smad2/3* expression disrupts formation of the node and its derivative the notochord. Finally, complete loss of *Smad2* and *Smad3* in the epiblast results in a failure to form middle streak lineages, including those that give rise to the bulk of the paraxial mesoderm and heart. By contrast, formation of posterior streak derivatives, including visceral yolk sac mesoderm and allantois, is a *Smad2/3*-independent process.

Homozygous *Smad2*$^{-/-}$; *Smad3*$^{-/-}$ double mutant embryos entirely lack mesodermal tissues

As shown above (Fig. 1), we observe *Smad2* and *Smad3* co-expression from the blastocyst stage onwards. Notably, by E5.5 *Smad2* and *Smad3* are both strongly expressed in the extra-embryonic ectoderm (Tremblay et al., 2000). To further evaluate their respective functional contributions, *Smad2*$^{Robm1/+}$;*Smad3*$^{null/+}$ double heterozygous mice were intercrossed. Four different phenotypic classes of embryos were recovered at late primitive streak stages, corresponding to: (1) overtly wild-type embryos, including *Smad2*$^{+/-}$;*Smad3*$^{+/+}$,

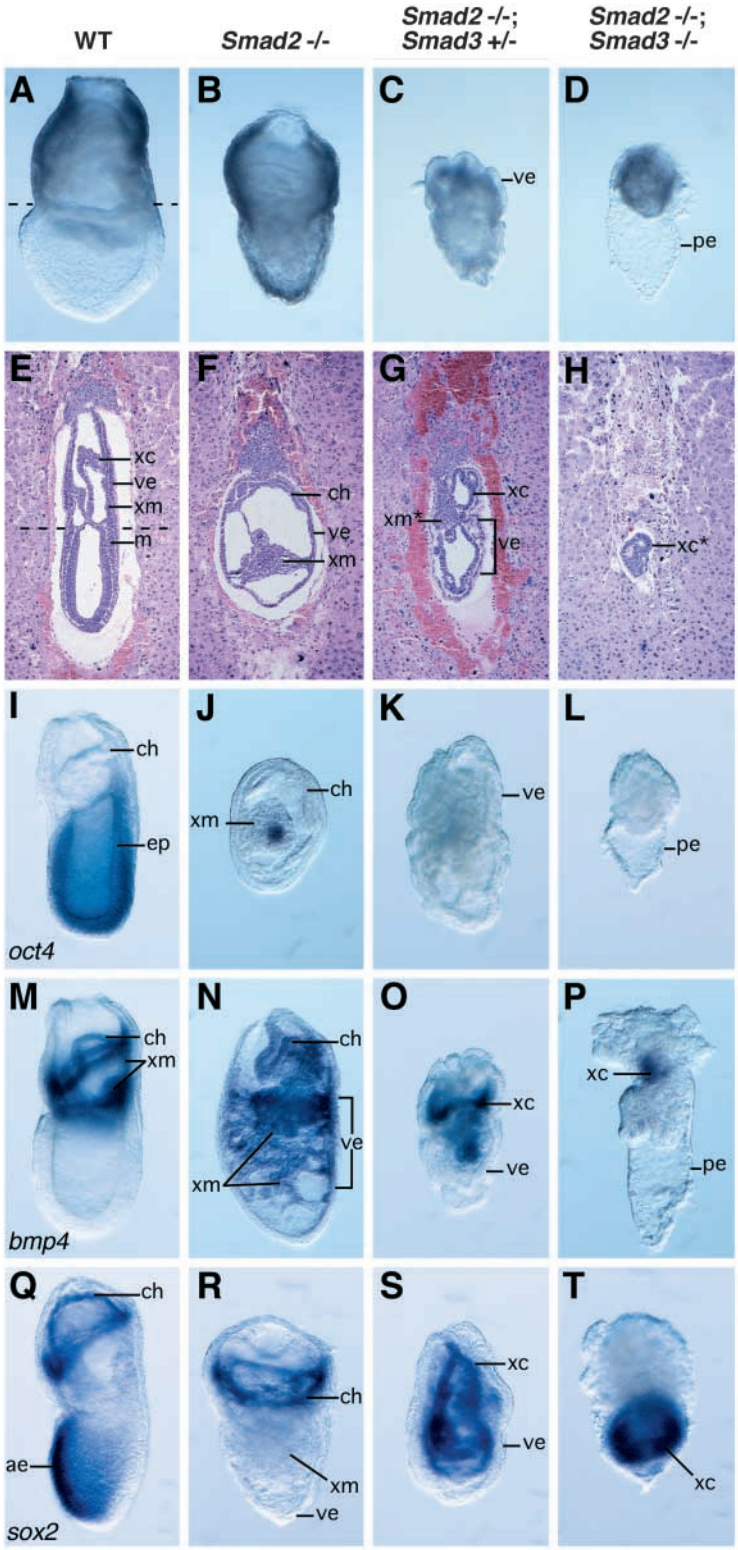

Fig. 6. Synergistic requirement for *Smad2* and *Smad3* in the patterning and organization of the early post-implantation embryo. Whole-mount views or transverse sections of embryos within the deciduum of E7.5 (A,E,I,M,Q) wild-type (WT; anterior towards the left), (B,F,J,N,R) *Smad2*$^{-/-}$, (C,G,K,O,S) *Smad2*$^{-/-}$;*Smad3*$^{+/-}$ and (D,H,L,P,T) *Smad2*$^{-/-}$;*Smad3*$^{-/-}$ embryos hybridized with (I-L) *Oct4*, (M-P) *Bmp4* or (Q-T) *Sox2* riboprobes. (A,E) Wild-type embryos have distinct embryonic and extra-embryonic regions (separated by broken line), with embryonic (m) (E) and *Bmp4*-expressing extra-embryonic (xm) mesoderm formation (E,M), and *Oct4*-expressing epiblast (ep) (I). (M) *Bmp4* and (Q) *Sox2* transcripts identify the extra-embryonic ectoderm (xc) (E) and its derivative the chorion (ch). *Smad2*$^{-/-}$ embryos express little *Oct4* (J) and form exclusively *Bmp4*-positive extra-embryonic mesoderm (F,N), which displaces the extra-embryonic ectoderm normally to form the chorion (ch) (F,J,N,R). *Smad2*$^{-/-}$;*Smad3*$^{+/-}$ mutant embryos undergo cavitation, but show no clear embryonic/extra-embryonic boundary, and are enveloped by a prominently folded and thickened layer of visceral endoderm (C,G,K,O,S) that surrounds disorganized extra-embryonic ectoderm (G,O,S), with little to no formation of presumptive extra-embryonic mesoderm (xm*) (G). (D,L,P,T) *Smad2*$^{-/-}$;*Smad3*$^{-/-}$ embryos develop as a small disorganized tissue mass within the parietal yolk sac endoderm (pe). Sections reveal rudimentary epithelial development with no mesoderm formation (H). Double mutants lack *Oct4* (L), but consistently show expression of *Bmp4* (P) and *Sox2* (T), suggesting loss of embryonic ectoderm and unique formation of extra-embryonic ectoderm (xc*) (H). ae, anterior ectoderm.

Smad2$^{+/-}$;*Smad3*$^{+/-}$ and *Smad2*$^{+/-}$;*Smad3*$^{-/-}$, which are unremarkable at this stage; (2) *Smad2*$^{-/-}$;*Smad3*$^{+/+}$ mutant embryos with defects described previously (Waldrip et al., 1998); (3) *Smad2*$^{-/-}$;*Smad3*$^{+/-}$ embryos; and (4) *Smad2*$^{-/-}$;*Smad3*$^{-/-}$ double mutants.

Smad2$^{-/-}$;*Smad3*$^{+/+}$ embryos fail to establish anterior pattern, and the epiblast gives rise exclusively to mesoderm that proliferates to form extra-embryonic structures including allantois and blood islands, as well as germ cells (Tremblay et al., 2001; Waldrip et al., 1998). We find that *Smad2*$^{-/-}$;*Smad3*$^{+/-}$ mutant embryos are more severely compromised and develop a distinct thickened rind of corrugated, prominently vacuolated columnar endoderm (Fig. 6C). Although cavitation occurs, we fail to observe a distinct boundary between extra-embryonic and embryonic regions (Fig. 6G). Rather the extra-embryonic ectoderm and epiblast are often folded and distorted, and only limited mesoderm formation is observed. Loss of pluripotential epiblast in these embryos was confirmed by analyzing expression of *Oct4*, which is normally robustly expressed at this stage of development (Fig. 6K,I). The identity of the presumptive extra-embryonic ectoderm and mesoderm populations was confirmed using *Sox2* and *Bmp4* (Fig. 6O,S).

Finally, we observe that *Smad2*$^{-/-}$;*Smad3*$^{-/-}$ double mutants closely resemble *Smad4*-deficient embryos (Sirard et al., 1998; Yang et al., 1998), show extremely limited development and are comprised of small masses of tissue within a normal parietal yolk sac (Fig. 6D). Histological analysis reveals no discernible boundary between the extra-embryonic ectoderm and the epiblast (Fig. 6H), and no mesoderm is present. In addition these double homozygous mutants lack *Oct4* expression (Fig. 6L). However *Sox2* and *Bmp4* transcripts are reproducibly detected, consistent with exclusive formation of extra-embryonic ectoderm (Fig. 6P,T). Thus, loss of Smad2/3 signals selectively

disrupts growth and patterning of the epiblast lineage of the egg cylinder stage embryo. Overall these experiments demonstrate that both Smad2 and Smad3 mediate cell fate decisions in the early post-implantation mouse embryo.

Discussion

Dose-dependent TGFβ/activin/Nodal signals play an essential role during early AP patterning of the vertebrate embryo (reviewed by Whitman, 2001). In the mouse, we recently described indistinguishable defects caused by conditional loss of *Smad2* or decreased *Nodal* expression in the epiblast (Vincent et al., 2003). These embryos fail to form axial mesendoderm and exhibit anterior patterning defects. Interestingly, a proportion of *Smad2*;*Nodal* double heterozygous embryos display similar anterior truncations (Nomura and Li, 1998). Thus, *Nodal/Smad2* signaling thresholds govern allocation of the axial mesendoderm precursors that selectively give rise to the ADE and PCP mesoderm.

Similar to Smad2, Smad3 elicits formation of dorsal mesoderm in *Xenopus* explant assays (Chen et al., 1997). Moreover, a variety of reporter assays implicates Smad2 and Smad3 functional redundancy. These findings raise the possibility that Smad3 also acts downstream of TGFβ/activin/Nodal signaling in the embryo. However, *Smad3* mutant mice develop normally and exhibit only subtle phenotypic abnormalities (Datto et al., 1999; Yang et al., 1999; Zhu et al., 1998). By contrast, *Smad2* mutant embryos develop early patterning defects because of a failure to establish the AVE (Brennan et al., 2001; Heyer et al., 1999; Waldrip et al., 1998). The simplest explanation to account for these distinct phenotypes is that Smad2 acts alone as the key transducer of TGFβ/activin/Nodal-related signals during early development. However, this is not the case. The present work demonstrates that (1) both Smad2 and Smad3 cooperate with the transcription factor Foxh1 to regulate the Foxh1-dependent autoregulatory enhancer present in the *Nodal* locus; (2) *Smad2* and *Smad3* as well as *Smad4* transcripts are expressed from the blastocyst stage onwards, with *Smad3* expression domains appearing more tightly regulated in comparison to widespread *Smad2* expression; (3) *Smad2* and *Smad3* expression ratios are independently regulated; and, finally, (4) combinatorial Smad2 and Smad3 activities indeed regulate mesoderm formation and patterning in the developing mouse embryo.

It has previously been shown that *Smad2* function in the epiblast is not required for establishment of the AVE, primitive streak formation or gastrulation movements (Tremblay et al., 2000; Waldrip et al., 1998). Rather selective loss of *Smad2* in the epiblast results in a failure to correctly specify progenitors of the AME (Vincent et al., 2003). Similarly, the AVE forms normally in $Smad2^{+/-}$;$Smad3^{-/-}$ embryos, and the anterior epiblast is endowed with neural pre-pattern. However, in this genetic context, loss of *Smad3* combined with decreased *Smad2* expression disrupts the production of anterior AME during gastrulation. Thus, we conclude that formation of the AME not only requires Smad2 but is also governed by the closely related molecule Smad3.

In the absence of anterior AME production during gastrulation, $Smad2^{+/-}$;$Smad3^{-/-}$ mutant embryos probably recruit extra-embryonic endoderm that fails to be displaced into a gut-like structure (Vincent et al., 2003). Consequently, the crucial refining signals that normally emanate from the anterior AME and orchestrate the continued patterning and morphogenesis of the anterior neuroectoderm are lost, and mutant embryos develop anterior truncations. The common origin, intimate morphogenesis and final topological proximity of the AME component tissues, the prechordal mesoderm and ADE, make it difficult to distinguish patterning activities contributed by these distinct cell populations. The divergent homeobox gene *Hhex* is specifically expressed in ADE, and chimeric embryos in which the ADE is largely *Hhex*-deficient show forebrain abnormalities (Martinez Barbera et al., 2000). By contrast, conditional disruption of *Foxa2* activity with *nestin:Cre* yields embryos that initially form, but fail to maintain the ADE and lack all other AME including prechordal mesoderm (Hallonet et al., 2002). Similar to $Smad2^{+/-}$;$Smad3^{-/-}$ mutants, conditional loss of *Foxa2* also results in severe anterior truncations and heart defects. Therefore, disrupting the morphogenesis or signaling by any single component of the anterior AME seems to impact the patterning activity of the remaining, tightly apposed cell lineage. Consistent with this idea, experiments in mice and chick have strongly implicated planar signaling within anterior midline tissues (Camus et al., 2000; Dale et al., 1997).

We further demonstrate that reduction in *Smad2/3* gene dose specifically within the epiblast sequentially eliminates anterior streak derivatives, first impacting the anterior AME ($Smad2^{Robm1/CA}$), then the node and remaining axial mesoderm ($Smad2^{Robm1/CA}$;$Smad3^{+/-}$), and finally affecting tissues that normally originate from the mid-streak including paraxial and lateral mesoderm ($Smad2^{Robm1/CA}$;$Smad3^{-/-}$). These experiments thus reveal a previously unappreciated role for Nodal-Smad2/3 signals in patterning middle primitive streak derivatives. Considering that *Foxh1*-null mutants display defects confined to the anterior streak (Hoodless et al., 2001; Yamamoto et al., 2001), we conclude these activities are mediated via Foxh1-independent pathways. Smad2 and Smad3 may therefore govern target gene expression by associating with other, yet to be described DNA-binding partners. Smad2/3 effectors may also regulate cellular responses by modulating intracellular components downstream of other signaling molecules. Indeed, considerable data demonstrate an interplay between TGFβ signaling pathways and those controlled by ERK/MAPK and EGF-Ras (reviewed by Derynck and Zhang, 2003; Shi and Massagué, 2003). Interestingly, disruption of FGF signaling leads to enhanced formation of axial mesoderm (Yamaguchi et al., 1994). A fine balance of signaling by TGFβ family members, FGFs and other growth factors seems to precisely control cell fate allocation in the primitive streak.

$Smad2^{-/-}$ embryos fail to form the AVE (Heyer et al., 1999; Waldrip et al., 1998). Consequently, anterior fates are not imposed on the epiblast. Rather, posteriorizing signals such as Bmp4 predominate and convert this tissue into nascent mesoderm that ultimately becomes specified to form extra-embryonic mesoderm and primordial germ cells (Lawson et al., 1999). We show that progressive reduction of *Smad3* expression in the context of *Smad2*-deficient embryos causes more severe phenotypes. Thus, mesoderm formation is greatly diminished in $Smad2^{-/-}$; $Smad3^{+/-}$ mutants, presumably as a result of highly reduced Nodal signaling within the epiblast (Brennan et al., 2001; Norris et al., 2002). Nonetheless, low

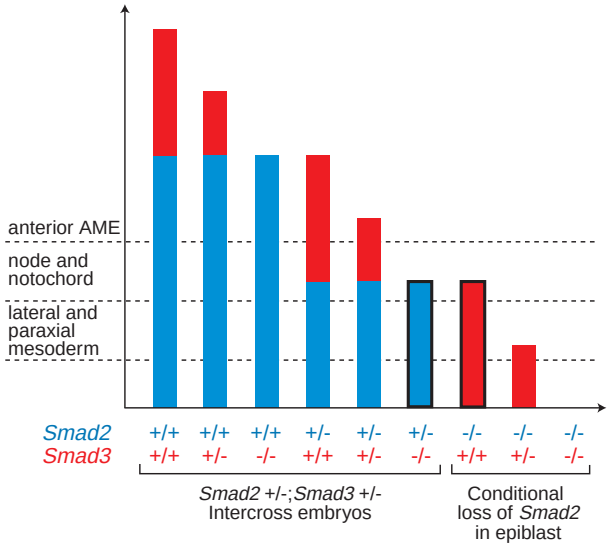

Fig. 7. Dose-dependent Smad2 and Smad3 signals pattern the primitive streak. Columns are grouped according to genotypes derived from intercrossing *Smad2*;*Smad3* double heterozygous mice (left) and specific elimination of *Smad2* in the epiblast in the context of progressive loss of *Smad3* (right). The identical phenotypes of $Smad2^{+/-}$;$Smad3^{-/-}$ and *Sox2Cre*;$Smad2^{CA/Robm1}$ mutant embryos (columns with black perimeter) suggest that Smad2 is the predominant intracellular effector of Nodal signaling during patterning of the primitive streak. This observation establishes the hypothetical dose relationship whereby one *Smad3* wild-type allele (red) is 50% less active than a *Smad2* wild-type allele (blue). Accordingly, the combined Smad2/3 dosage is then calculated for each genotype analyzed in our studies. Three phenotypic thresholds emerge below which patterning of the primitive streak is sequentially compromised. The first eliminates the anterior AME followed by the node, remaining axial mesoderm (notochord) and definitive endoderm, and finally the lateral and paraxial mesoderm.

levels of Nodal appear to promote maintenance of the adjacent extra-embryonic ectoderm, and this tissue as well as the visceral endoderm appears to proliferate normally (Fig. 5).

$Smad2^{-/-}$;$Smad3^{-/-}$ embryos are even more severely compromised. We observe minimal elaboration of the embryonic and extra-embryonic cell populations, and mesoderm induction is entirely absent. Interestingly, these double mutant embryos closely resemble *Smad4*-deficient or *ActRIIA*/*IIB*-doubly deficient embryos, and are consistently smaller than *Nodal* mutant embryos (Sirard et al., 1998; Song et al., 1999; Yang et al., 1998). It is tempting to speculate that TGFβ-family members secreted by the maternal decidual tissue and acting upstream of Smad2/3, such as activin, collaborate with Nodal to promote growth and organization of the early embryonic and extra-embryonic lineages.

The genotypes and corresponding tissue disturbances generated by intercrossing $Smad2^{Robm1/+}$ and $Smad3^{null/+}$ mutant mice are summarized in Fig. 7. The striking phenotypic similarity shared between $Smad2^{+/-}$;$Smad3^{-/-}$ embryos and those selectively lacking Smad2 activity in the epiblast ($Smad2^{Robm1/CA}$;*Sox2Cre*) suggests that functions mediated by one copy of *Smad2* are roughly equivalent to those provided by wild-type levels of *Smad3*. If the combined levels of Smad2 and Smad3 activities within cells of the epiblast and primitive streak fall below a crucial threshold level, formation of anterior AME is eliminated. The fact that *Smad2*;*Smad3* double heterozygous animals develop normally defines the upper limit of this threshold. Progressive loss of *Smad3* in the context of a *Smad2*-deficient epiblast eventually disrupts node and axial mesoderm formation. Further reduction of Smad2/3 signals compromises paraxial and lateral mesoderm formation (Fig. 7). The simplest explanation to account for the relatively strong *Smad2* gene dose effects is that Smad2 is more abundant in the early embryo. RPA experiments indeed reveal approximately twofold higher levels of *Smad2* transcripts in early gastrulation stage embryos (Fig. 1), which is consistent with the less robust expression of *Smad3* in zebrafish and *Xenopus* gastrula-stage embryos (Dick et al., 2000; Howell et al., 2001). Interestingly surveys of Smad2 and Smad3 protein distribution using cross-reactive antibodies reveals that Smad2 is more broadly expressed, whereas Smad3 shows a more restricted pattern in embryos, tissues and cell lines (Flanders et al., 2001) (N.R.D., S.D.V., L.O., E.J.R. and E.K.B., unpublished). Smad3 may therefore amplify Smad2 signals in selected cell types.

Post-transcriptional and/or -translational stability, differential targeting for ubiquitin-mediated degradation, as well as the efficiency of nucleocytoplasmic shuttling may further modulate shared and/or unique Smad2/3 activities. Our genetic findings are all the more striking because functional differences between Smad2 and Smad3 have been extensively documented, albeit in cultured cell lines. Finally, an additional layer of complexity comes from the observation that *Smad2* is alternatively spliced in vertebrates. The shorter, less predominant isoform more closely resembles Smad3, and exhibits identical biochemical properties (Dennler et al., 1999; Yagi et al., 1999). An interesting possibility is that dynamic cellular responses of discrete target cell subpopulations is modulated by shifting ratios of Smad2 to Smad3-like activities.

We thank Chad Koonce, Dorian Anderson, Rebecca Kim and Ayesha Islam for technical support; and Debbie Pelusi for genotyping assistance. We are grateful to Xiao-fan Wang for kindly providing *Smad3* null mice; and to Liliana Attisano, Mark de Caestecker, Gerald Chu, Hiroshi Hamada, Masahiro Kawabata, Jun-ichi Miyazaki and Jeff Wrana for plasmid reagents and protocols. N.R.D. was supported by a post-doctoral fellowship from the NICHD, S.D.V. was supported by a Long Term Fellowship from the HFSP and L.O. was supported by a postdoctoral fellowship from the Medical Foundation of Boston. This work was supported by grants from the NIH.

References

Adachi, H., Saijoh, Y., Mochida, K., Ohishi, S., Hashiguchi, H., Hirao, A. and Hamada, H. (1999). Determination of left/right asymmetric expression of Nodal by a left side-specific enhancer with sequence similarity to a lefty-2 enhancer. *Genes Dev.* **13**, 1589-1600.

Bachiller, D., Klingensmith, J., Kemp, C., Belo, J. A., Anderson, R. M., May, S. R., McMahon, J. A., McMahon, A. P., Harland, R. M., Rossant, J. et al. (2000). The organizer factors Chordin and Noggin are required for mouse forebrain development. *Nature* **403**, 658-661.

Baker, J. C. and Harland, R. M. (1996). A novel mesoderm inducer, Madr2, functions in the activin signal transduction pathway. *Genes Dev.* **10**, 1880-1889.

Balemans, W. and van Hul, W. (2002). Extracellular regulation of BMP signaling in vertebrates: a cocktail of modulators. *Dev. Biol.* **250**, 231-250.

Brennan, J., Lu, C. C., Norris, D. P., Rodriguez, T. A., Beddington, R. S. and Robertson, E. J. (2001). Nodal signalling in the epiblast patterns the early mouse embryo. *Nature* **411**, 965-969.

Camus, A., Davidson, B. P., Billiards, S., Khoo, P., Rivera-Perez, J. A.,

Wakamiya, M., Behringer, R. R. and Tam, P. P. (2000). The morphogenetic role of midline mesendoderm and ectoderm in the development of the forebrain and the midbrain of the mouse embryo. *Development* **127**, 1799-1813.

Camus, A. and Tam, P. P. L. (1999). The organizer of the gastrulating mouse embryo. *Curr. Top. Dev. Biol.* **45**, 117-153.

Chen, Y. and Schier, A. F. (2001). The zebrafish Nodal signal Squint functions as a morphogen. *Nature* **411**, 607-610.

Chen, Y., Bhushan, A. and Vale, W. (1997). Smad8 mediates the signaling of the ALK-2 receptor serine kinase. *Proc. Natl. Acad. Sci. USA* **94**, 12938-12943.

Conlon, F. L., Barth, K. S. and Robertson, E. J. (1991). A novel retrovirally induced embryonic lethal mutation in the mouse: assessment of the developmental fate of embryonic stem cells homozygous for the 413.d proviral integration. *Development* **111**, 969-981.

Conlon, F. L., Lyons, K. M., Takaesu, N., Barth, K. S., Kispert, A., Herrmann, B. and Robertson, E. J. (1994). A primary requirement for Nodal in the formation and maintenance of the primitive streak in the mouse. *Development* **120**, 1919-1928.

Dale, J. K., Vesque, C., Lints, T. J., Sampath, T. K., Furley, A., Dodd, J. and Placzek, M. (1997). Cooperation of BMP7 and SHH in the induction of forebrain ventral midline cells by prechordal mesoderm. *Cell* **90**, 257-269.

Datto, M. B., Frederick, J. P., Pan, L., Borton, A. J., Zhuang, Y. and Wang, X. F. (1999). Targeted disruption of Smad3 reveals an essential role in transforming growth factor beta-mediated signal transduction. *Mol. Cell Biol.* **19**, 2495-2504.

de Sousa Lopes, S. M., Carvalho, R. L., van den Driesche, S., Goumans, M. J., ten Dijke, P. and Mummery, C. L. (2003). Distribution of phosphorylated Smad2 identifies target tissues of TGFbeta ligands in mouse development. *Gene Expr. Patt.* **3**, 355-360.

Dennler, S., Huet, S. and Gauthier, J. M. (1999). A short amino-acid sequence in MH1 domain is responsible for functional differences between Smad2 and Smad3. *Oncogene* **18**, 1643-1648.

Derynck, R. and Zhang, Y. E. (2003). Smad-dependent and Smad-independent pathways in TGF-beta family signalling. *Nature* **425**, 577-584.

Dick, A., Mayr, T., Bauer, H., Meier, A. and Hammerschmidt, M. (2000). Cloning and characterization of zebrafish smad2, smad3 and smad4. *Gene* **246**, 69-80.

Dunn, N. R., Winnier, G. E., Hargett, L. K., Schrick, J. J., Fogo, A. B. and Hogan, B. L. M. (1997). Haploinsufficient phenotypes in Bmp4 heterozygous null mice and modification by mutations in Gli3 and Alx4. *Dev. Biol.* **188**, 235-247.

Flanders, K. C., Kim, E. S. and Roberts, A. B. (2001). Immunohistochemical expression of Smads 1-6 in the 15-day gestation mouse embryo: signaling by BMPs and TGF-betas. *Dev. Dyn.* **220**, 141-154.

Graff, J. M., Bansal, A. and Melton, D. A. (1996). Xenopus Mad proteins transduce distinct subsets of signals for the TGF beta superfamily. *Cell* **85**, 479-487.

Green, M. C. (1968). Mechanism of the pleiotropic effects of the short-ear mutant gene in the mouse. *J. Exp. Zool.* **167**, 129-150.

Hallonet, M., Kaestner, K. H., Martin-Parras, L., Sasaki, H., Betz, U. A. and Ang, S. L. (2002). Maintenance of the specification of the anterior definitive endoderm and forebrain depends on the axial mesendoderm: a study using HNF3beta/Foxa2 conditional mutants. *Dev. Biol.* **243**, 20-33.

Heyer, J., Escalante-Alcalde, D., Lia, M., Boettinger, E., Edelmann, W., Stewart, C. L. and Kucherlapati, R. (1999). Postgastrulation Smad2-deficient embryos show defects in embryo turning and anterior morphogenesis. *Proc. Natl. Acad. Sci. USA* **96**, 12595-12600.

Hogan, B. L. M. (1996). Bone morphogenetic proteins: multifunctional regulators of vertebrate development. *Genes Dev.* **10**, 1580-1594.

Hoodless, P. A., Pye, M., Chazaud, C., Labbe, E., Attisano, L., Rossant, J. and Wrana, J. L. (2001). FoxH1 (Fast) functions to specify the anterior primitive streak in the mouse. *Genes Dev.* **15**, 1257-1271.

Howell, M., Mohun, T. J. and Hill, C. S. (2001). Xenopus Smad3 is specifically expressed in the chordoneural hinge, notochord and in the endocardium of the developing heart. *Mech. Dev.* **104**, 147-150.

Kumar, A., Novoselov, V., Celeste, A. J., Wolfman, N. M., ten Dijke, P. and Kuehn, M. R. (2001). Nodal signaling uses activin and transforming growth factor-beta receptor-regulated Smads. *J. Biol. Chem.* **276**, 656-661.

Labbé, E., Silvestri, C., Hoodless, P. A., Wrana, J. L. and Attisano, L. (1998). Smad2 and Smad3 positively and negatively regulate TGF beta-dependent transcription through the forkhead DNA-binding protein FAST2. *Mol. Cell* **2**, 109-120.

Lawson, K. A. (1999). Fate mapping the mouse embryo. *Int. J. Dev. Biol.* **43**, 773-775.

Lawson, K. A., Dunn, N. R., Roelen, B. A., Zeinstra, L. M., Davis, A. M., Wright, C. V. E., Korving, J. P. and Hogan, B. L. M. (1999). Bmp4 is required for the generation of primordial germ cells in the mouse embryo. *Genes Dev.* **13**, 424-436.

Lebrun, J. J., Takabe, K., Chen, Y. and Vale, W. (1999). Roles of pathway-specific and inhibitory Smads in activin receptor signaling. *Mol. Endocrinol.* **13**, 15-23.

Liu, F. (2003). Receptor-regulated Smads in TGF-beta signaling. *Front. Biosci.* **8**, S1280-S1303.

Lowe, L. A., Yamada, S. and Kuehn, M. R. (2001). Genetic dissection of Nodal function in patterning the mouse embryo. *Development* **128**, 1831-1843.

Martinez Barbera, J. P., Clements, M., Thomas, P., Rodriguez, T., Meloy, D., Kioussis, D. and Beddington, R. S. P. (2000). The homeobox gene Hex is required in definitive endodermal tissues for normal forebrain, liver and thyroid formation. *Development* **127**, 2433-2445.

Massagué, J. and Wotton, D. (2000). Transcriptional control by the TGF-beta/Smad signaling system. *EMBO J.* **19**, 1745-1754.

Moustakas, A., Souchelnytskyi, S. and Heldin, C. H. (2001). Smad regulation in TGF-beta signal transduction. *J. Cell Sci.* **114**, 4359-4369.

Nagy, A., Gertsentein, M., Vintersten, K. and Behringer, R. (2003). *Manipulating the Mouse Embryo*. New York: Cold Spring Harbor Laboratory Press.

Niwa, H., Yamamura, K. and Miyazaki, J. (1991). Efficient selection for high-expression transfectants with a novel eukaryotic vector. *Gene* **108**, 193-199.

Nomura, M. and Li, E. (1998). Smad2 role in mesoderm formation, left-right patterning and craniofacial development. *Nature* **393**, 786-790.

Norris, D. P., Brennan, J., Bikoff, E. K. and Robertson, E. J. (2002). The Foxh1-dependent autoregulatory enhancer controls the level of Nodal signals in the mouse embryo. *Development* **129**, 3455-3468.

Norris, D. P. and Robertson, E. J. (1999). Asymmetric and node-specific Nodal expression patterns are controlled by two distinct cis-acting regulatory elements. *Genes Dev.* **13**, 1575-1588.

Oxburgh, L. and Robertson, E. J. (2002). Dynamic regulation of Smad expression during mesenchyme to epithelium transition in the metanephric kidney. *Mech. Dev.* **112**, 207-211.

Reissmann, E., Jornvall, H., Blokzijl, A., Andersson, O., Chang, C., Minchiotti, G., Persico, M. G., Ibanez, C. F. and Brivanlou, A. H. (2001). The orphan receptor ALK7 and the Activin receptor ALK4 mediate signaling by Nodal proteins during vertebrate development. *Genes Dev.* **15**, 2010-2022.

Rosendahl, A., Checchin, D., Fehniger, T. E., ten Dijke, P., Heldin, C. H. and Sideras, P. (2001). Activation of the TGF-beta/activin-Smad2 pathway during allergic airway inflammation. *Am. J. Respir. Cell Mol. Biol.* **25**, 60-68.

Rubenstein, J. L., Shimamura, K., Martinez, S. and Puelles, L. (1998). Regionalization of the prosencephalic neural plate. *Annu. Rev. Neurosci.* **21**, 445-477.

Saijoh, Y., Adachi, H., Sakuma, R., Yeo, C. Y., Yashiro, K., Watanabe, M., Hashiguchi, H., Mochida, K., Ohishi, S., Kawabata, M. et al. (2000). Left-right asymmetric expression of lefty2 and Nodal is induced by a signaling pathway that includes the transcription factor FAST2. *Mol. Cell* **5**, 35-47.

Schier, A. F. and Shen, M. M. (2000). Nodal signalling in vertebrate development. *Nature* **403**, 385-389.

Shawlot, W., Wakamiya, M., Kwan, K. M., Kania, A., Jessell, T. M. and Behringer, R. R. (1999). Lim1 is required in both primitive streak-derived tissues and visceral endoderm for head formation in the mouse. *Development* **126**, 4925-4932.

Shi, Y. and Massagué, J. (2003). Mechanisms of TGF-beta signaling from cell membrane to the nucleus. *Cell* **113**, 685-700.

Shi, Y., Wang, Y. F., Jayaraman, L., Yang, H., Massagué, J. and Pavletich, N. P. (1998). Crystal structure of a Smad MH1 domain bound to DNA: insights on DNA binding in TGF-beta signaling. *Cell* **94**, 585-594.

Sirard, C., de la Pompa, J. L., Elia, A., Itie, A., Mirtsos, C., Cheung, A., Hahn, S., Wakeham, A., Schwartz, L., Kern, S. E. et al. (1998). The tumor suppressor gene Smad4/Dpc4 is required for gastrulation and later for anterior development of the mouse embryo. *Genes Dev.* **12**, 107-119.

Song, J., Oh, S. P., Schrewe, H., Nomura, M., Lei, H., Okano, M., Gridley, T. and Li, E. (1999). The type II activin receptors are essential for egg cylinder growth, gastrulation, and rostral head development in mice. *Dev. Biol.* **213**, 157-169.

Stern, C. D. (2001). Initial patterning of the central nervous system: how many organizers? *Nat. Rev. Neurosci.* **2**, 92-98.

Tremblay, K. D., Hoodless, P. A., Bikoff, E. K. and Robertson, E. J. (2000). Formation of the definitive endoderm in mouse is a Smad2-dependent process. *Development* **127**, 3079-3090.

Tremblay, K. D., Dunn, N. R. and Robertson, E. J. (2001). Mouse embryos lacking Smad1 signals display defects in extra-embryonic tissues and germ cell formation. *Development* **128**, 3609-3621.

Varlet, I., Collignon, J. and Robertson, E. J. (1997). Nodal expression in the primitive endoderm is required for specification of the anterior axis during mouse gastrulation. *Development* **124**, 1033-1044.

Vincent, S. D., Dunn, N. R., Hayashi, S., Norris, D. P. and Robertson, E. J. (2003). Cell fate decisions within the mouse organizer are governed by graded Nodal signals. *Genes Dev.* **17**, 1646-1662.

Waldrip, W. R., Bikoff, E. K., Hoodless, P. A., Wrana, J. L. and Robertson, E. J. (1998). Smad2 signaling in extraembryonic tissues determines anterior-posterior polarity of the early mouse embryo. *Cell* **92**, 797-808.

Weinstein, M., Monga, S. P., Liu, Y., Brodie, S. G., Tang, Y., Li, C., Mishra, L. and Deng, C. X. (2001). Smad proteins and hepatocyte growth factor control parallel regulatory pathways that converge on beta1-integrin to promote normal liver development. *Mol. Cell Biol.* **21**, 5122-5131.

Whitman, M. (1998). Smads and early developmental signaling by the TGFbeta superfamily. *Genes Dev.* **12**, 2445-2462.

Whitman, M. (2001). Nodal signaling in early vertebrate embryos: themes and variations. *Dev. Cell* **1**, 605-617.

Yagi, K., Goto, D., Hamamoto, T., Takenoshita, S., Kato, M. and Miyazono, K. (1999). Alternatively spliced variant of Smad2 lacking exon 3. Comparison with wild-type Smad2 and Smad3. *J. Biol. Chem.* **274**, 703-709.

Yamaguchi, T. P., Harpal, K., Henkemeyer, M. and Rossant, J. (1994). fgfr-1 is required for embryonic growth and mesodermal patterning during mouse gastrulation. *Genes Dev.* **8**, 3032-3044.

Yamamoto, M., Meno, C., Sakai, Y., Shiratori, H., Mochida, K., Ikawa, Y., Saijoh, Y. and Hamada, H. (2001). The transcription factor FoxH1 (FAST) mediates Nodal signaling during anterior-posterior patterning and node formation in the mouse. *Genes Dev.* **15**, 1242-1256.

Yang, X., Li, C., Xu, X. and Deng, C. (1998). The tumor suppressor SMAD4/DPC4 is essential for epiblast proliferation and mesoderm induction in mice. *Proc. Natl. Acad. Sci. USA* **95**, 3667-3672.

Yang, X., Letterio, J. J., Lechleider, R. J., Chen, L., Hayman, R., Gu, H., Roberts, A. B. and Deng, C. (1999). Targeted disruption of SMAD3 results in impaired mucosal immunity and diminished T cell responsiveness to TGF-beta. *EMBO J.* **18**, 1280-1291.

Yeo, C. Y., Chen, X. and Whitman, M. (1999). The role of FAST-1 and Smads in transcriptional regulation by activin during early Xenopus embryogenesis. *J. Biol. Chem.* **274**, 26584-26590.

Zhao, G. Q. (2003). Consequences of knocking out BMP signaling in the mouse. *Genesis* **35**, 43-56.

Zhu, Y., Richardson, J. A., Parada, L. F. and Graff, J. M. (1998). Smad3 mutant mice develop metastatic colorectal cancer. *Cell* **94**, 703-714.